

Fundamental limits on the rate of bacterial cell division

Nathan M. Belliveau^{†, 1}, Griffin Chure^{†, 2, 3}, Christina L. Hueschen⁴, Hernan G. Garcia⁵, Jané Kondev⁶, Daniel S. Fisher⁷, Julie Theriot^{1, 8}, Rob Phillips^{2, 9,*}

*For correspondence:

[†]These authors contributed equally to this work

¹Department of Biology, University of Washington, Seattle, WA, USA; ²Division of Biology and Biological Engineering, California Institute of Technology, Pasadena, CA, USA; ³Department of Applied Physics, California Institute of Technology, Pasadena, CA, USA; ⁴Department of Chemical Engineering, Stanford University, Stanford, CA, USA; ⁵Department of Molecular Cell Biology and Department of Physics, University of California Berkeley, Berkeley, CA, USA; ⁶Department of Physics, Brandeis University, Waltham, MA, USA; ⁷Department of Applied Physics, Stanford University, Stanford, CA, USA; ⁸Allen Institute for Cell Science, Seattle, WA, USA; ⁹Department of Physics, California Institute of Technology, Pasadena, CA, USA; *Contributed equally

Abstract

Introduction

The range of bacterial growth rates is enormously diverse. In natural environments, some microbial organisms might double only once per year while in comfortable laboratory conditions, growth can be rapid with several divisions per hour. This six order of magnitude difference illustrates the intimate relationship between environmental conditions and the rates at which cells convert nutrients into new cellular material – a relationship that has remained a major topic of inquiry in bacterial physiology for over a century (*Jun et al., 2018*). As was noted by Jacques Monod, “the study of the growth of bacterial cultures does not constitute a specialized subject or branch of research, it is the basic method of Microbiology.” Those words ring as true today as they did when they were written 70 years ago. Indeed, the study of bacterial growth has undergone a molecular resurgence since many of the key questions addressed by the pioneering efforts in the middle of the last century can be revisited by examining them through the lens of the increasingly refined molecular census that is available for bacteria such as the microbial workhorse *Escherichia coli*. Several of the outstanding questions that can now be studied about bacterial growth include: what sets the fastest time scale that bacteria can divide, and how is growth rate tied to the quality of the carbon source. In this paper, we address these two questions from two distinct angles. First, as a result of an array of high-quality proteome-wide measurements of the *E. coli* proteome under a myriad of different growth conditions, we have a census that allows us to explore how the number of key molecular players change as a function of growth rate. This census provides a window onto whether the processes they mediate such as molecular transport into the cells and molecular synthesis within cells can run faster. Second, because of our understanding of the molecular pathways responsible for many of the steps in bacterial growth, we can also make order of magnitude estimates to infer the copy numbers that would be needed to achieve a given growth rate. In this paper, we pass back and forth between the analysis of a variety of different proteomic datasets and order-of-magnitude estimations to determine possible molecular bottlenecks that limit bacterial growth and to see how

42 the growth rate varies in different carbon sources.

43 Specifically, we leverage a combination of *E. coli* proteomic data sets collected over the past
 44 decade using either mass spectrometry (*Schmidt et al., 2016; Peebo et al., 2015; Valgepea et al.,*
 45 **2013**) or ribosomal profiling (*Li et al., 2014*) across 31 unique growth conditions. Broadly speaking,
 46 we entertain several classes of hypotheses as are illustrated in **Figure 1**. First, we consider potential
 47 limits on the transport of nutrients into the cell. We address this hypothesis by performing an
 48 order-of-magnitude estimate for how many carbon, phosphorous, and sulfur atoms are needed to
 49 facilitate this requirement given a 5000 second division time. As a second hypothesis, we consider
 50 the possibility that there exists a fundamental limit on how quickly the cell can generate ATP. We
 51 approach this hypothesis from two angles, considering how many ATP synthase complexes must
 52 be needed to churn out enough ATP to power protein translation followed by an estimation of
 53 how many electron transport complexes must be present to maintain the proton motive force.
 54 A third class of estimates considers the need to maintain the size and shape of the cell through
 55 the construction of new lipids for the cell membranes as well as the glycan polymers which make
 56 up the rigid peptidoglycan. Our final class of hypotheses centers on the synthesis of a variety of
 57 biomolecules. Our focus is primarily on the stages of the central dogma as we estimate the number
 58 of protein complexes needed for DNA replication, transcription, and protein translation.

59 In broad terms, we find that the majority of these estimates are in close agreement with the
 60 experimental observations, with protein copy numbers apparently well-tuned for the task of cell
 61 doubling. This allows us to systematically scratch off the hypotheses diagrammed in **Figure 1** as
 62 setting possible speed limits. Ultimately, we find that protein translation (particularly the generation
 63 of new ribosomes) acts as 1) a rate limiting step for the *fastest* bacterial division, and 2) the major
 64 determinant of bacterial growth across all nutrient conditions we have considered under steady
 65 state, exponential growth. This perspective is in line with the linear correlation observed between
 66 growth rate and ribosomal content (typically quantified through the ratio of RNA to protein) for fast
 67 growing cells (*Scott et al., 2010*), but suggests a more prominent role for ribosomes in setting the
 68 doubling time across all conditions of nutrient limitation. Here we again leverage the quantitative
 69 nature of this data set and present a quantitative model of the relationship between the fraction of
 70 the proteome devoted to ribosomes and the speed limit of translation, revealing a fundamental
 71 tradeoff between the translation capacity of the ribosome pool and the maximal growth rate.

72 Uptake of Nutrients

73 In order to build new cellular mass, the molecular and elemental building blocks must be scavenged
 74 from the environment in different forms. Carbon, for example, is acquired via the transport of
 75 carbohydrates and sugar alcohols with some carbon sources receiving preferential treatment
 76 in their consumption (*Monod, 1947*). Phosphorus, sulfur, and nitrogen, on the other hand, are
 77 harvested primarily in the forms of inorganic salts, namely phosphate, sulfate, and ammonia
 78 (*Jun et al., 2018; Assentoft et al., 2016; Stasi et al., 2019; Antonenko et al., 1997; Rosenberg et al.,*
 79 **1977; Willsky et al., 1973**). All of these compounds have different permeabilities across the cell
 80 membrane and most require some energetic investment either via ATP hydrolysis or through the
 81 proton electrochemical gradient to bring the material across the hydrophobic cell membrane. Given
 82 the diversity of biological transport mechanisms and the vast number of inputs needed to build a
 83 cell, we begin by considering transport of some of the most important cellular ingredients: carbon,
 84 nitrogen, oxygen, hydrogen, phosphorus, and sulfur.

85 The elemental composition of *E. coli* has received much quantitative attention over the past
 86 half century (*Neidhardt et al., 1991; Taymaz-Nikerel et al., 2010; Heldal et al., 1985; Bauer and Ziv,*
 87 **1976**), providing us with a starting point for estimating the copy numbers of various transporters.
 88 While there is some variability in the exact elemental percentages (with different uncertainties), we
 89 can estimate that the dry mass of a typical *E. coli* cell is \approx 45% carbon (BNID: 100649, *Milo et al.*
 90 **(2010)**), \approx 15% nitrogen (BNID: 106666, *Milo et al. (2010)*), \approx 3% phosphorus (BNID: 100653, *Milo*
 91 **et al. (2010)**), and 1% sulfur (BNID: 100655, *Milo et al. (2010)*). In the coming paragraphs, we will

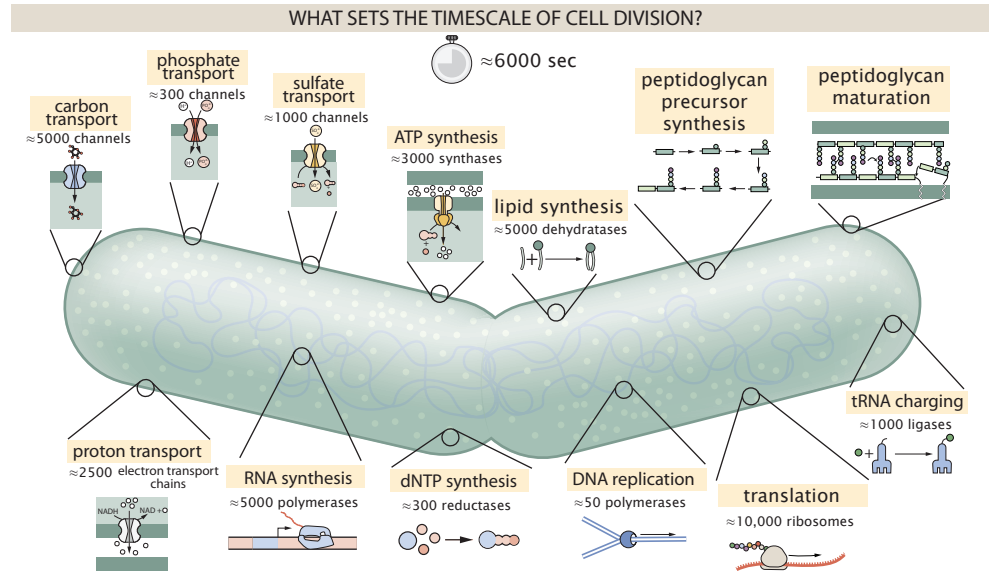


Figure 1. Transport and synthesis processes necessary for cell division. We consider an array of processes necessary for a cell to double its molecular components. Such processes include the transport of carbon across the cell membrane, the production of ATP, and fundamental processes of the central dogma namely RNA, DNA, and protein synthesis. A schematic of each synthetic or transport category is shown with an approximate measure of the complex abundance at a growth rate of 0.5 per hour. In this work, we consider a standard bacterial division time of ≈ 5000 sec.

92 engage in a dialogue between back-of-the-envelope estimates for the numbers of transporters
 93 needed to facilitate these chemical stoichiometries and the experimental proteomic measurements
 94 of the biological reality. Such an approach provides the opportunity to test if our biological knowl-
 95 edge is sufficient to understand the scale at which these complexes are produced. Specifically, we
 96 will make these estimates considering a modest doubling time of 5000 s, a growth rate of $\approx 0.5 \text{ hr}^{-1}$,
 97 the range in which the majority of the experimental measurements reside.

98 Carbon Transport

99 We begin with the most abundant element by mass, carbon. Using $\approx 0.3 \text{ pg}$ as the typical *E. coli*
 100 dry mass (BNID: 103904, *Milo et al. (2010)*), we estimate that $\approx 10^{10}$ carbon atoms must be brought
 101 into the cell in order to double all of the carbon-containing molecules (*Figure 2(A, top)*). Typical
 102 laboratory growth conditions, such as those explored in the aforementioned proteomic data sets,
 103 provide carbon as a single class of sugar such as glucose, galactose, or xylose to name a few. *E.*
 104 *coli* has evolved myriad mechanisms by which these sugars can be transported across the cell
 105 membrane. One such mechanism of transport is via the PTS system which is a highly modular
 106 system capable of transporting a diverse range of sugars (*Escalante et al., 2012*). The glucose-
 107 specific component of this system transports ≈ 200 glucose molecules per second per channel
 108 (BNID: 114686, *Milo et al. (2010)*). Making the assumption that this is a typical sugar transport rate,
 109 coupled with the need to transport 10^{10} carbon atoms, we arrive at the conclusion that on the order
 110 of 1,000 transporters must be expressed in order to bring in enough carbon atoms to divide in
 111 6,000 s, diagrammed in the top panel of *Figure 2(A)*. This estimate, along with the observed average
 112 number of carbohydrate transporters present in the proteomic data sets (*Schmidt et al., 2016*;
 113 *Peebo et al., 2015; Valgepea et al., 2013; Li et al., 2014*), is shown in *Figure 2(A)*. While we estimate
 114 1,000 transporters are needed, the data reveals that at a division time of ≈ 5000 s there is nearly
 115 a ten-fold excess of transporters. Furthermore, the data illustrates that the average number of
 116 carbohydrate transporters present is largely-growth rate independent.

117 The estimate presented in *Figure 2(A)* neglects any specifics of the regulation of carbon transport

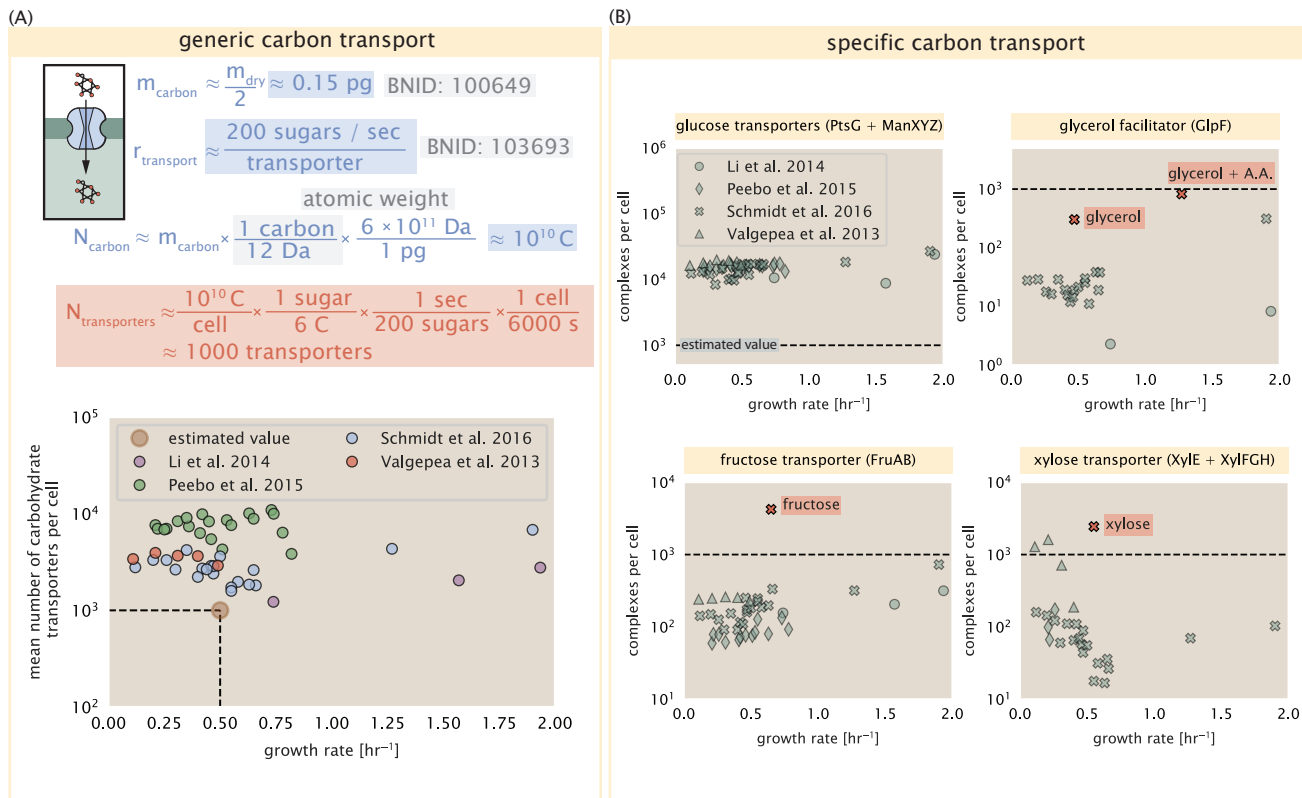


Figure 2. The abundance of carbon transport systems across growth rates. (A) A simple estimate for the minimum number of generic carbohydrate transport systems (top) assumes $\approx 10^{10}$ C are needed to complete division, each transported sugar contains ≈ 6 C, and each transporter conducts sugar molecules at a rate of ≈ 200 per second. Bottom plot shows the estimated number of transporters needed at a growth rate of ≈ 0.5 per hr (light-brown point and dashed lines). Colored points correspond to the mean number of carbohydrate transporters for different growth conditions across different published datasets. (B) The abundance of various specific carbon transport systems plotted as a function of the population growth rate. Red points and red-highlighted text indicate conditions in which the only source of carbon in the growth medium induces expression of the transport system.

118 system and presents a data-averaged view of how many carbohydrate transporters are present
 119 on average. Using the diverse array of growth conditions explored in the proteomic data sets, we
 120 can explore how individual carbon transport systems depend on the population growth rate. In
 121 **Figure 2(B)**, we show the total number of carbohydrate transporters specific to different carbon
 122 sources. A striking observation, shown in the top-left plot of **Figure 2(B)**, is the constancy in the
 123 expression of the glucose-specific transport systems (the PtsG enzyme of the PTS system and the
 124 glucose-transporting ManXYZ complex). Additionally, we note that the total number of glucose-
 125 specific transporters is tightly distributed $\approx 10^4$ per cell, an order of magnitude beyond the estimate
 126 shown in **Figure 2(A)**. This illustrates that *E. coli* maintains a substantial number of complexes
 127 present for transporting glucose which is known to be the preferential carbon source (**Monod, 1947**;
 128 **Liu et al., 2005; Aidelberg et al., 2014**).

129 It is now understood that a large number of metabolic operons are regulated with dual-input
 130 logic gates that are only expressed when glucose concentrations are low (mediated by cyclic-AMP
 131 receptor protein CRP) and the concentration of other carbon sources are elevated (**Gama-Castro**
 132 *et al.*, 2016; **Zhang et al.**, 2014b). A famed example of such dual-input regulatory logic is in the
 133 regulation of the *lac* operon which is only natively activated in the absence of glucose and the
 134 presence of allolactose, an intermediate in lactose metabolism (**Jacob and Monod, 1961**), though we
 135 now know of many other such examples (**Ireland et al.**, 2020; **Gama-Castro et al.**, 2016; **Belliveau**
 136 *et al.*, 2018). This illustrates that once glucose is depleted from the environment, cells have a means
 137 to dramatically increase the abundance of the specific transporter needed to digest the next sugar
 138 that is present. Several examples of induced expression of specific carbon-source transporters
 139 are shown in **Figure 2(B)**. Points colored in red (labeled by red text-boxes) correspond to growth
 140 conditions in which the specific carbon source (glycerol, xylose, or fructose) is present. These
 141 plots show that, in the absence of the particular carbon source, expression of the transporters is
 142 maintained on the order of $\sim 10^2$ per cell. However, when induced, the transporters become highly-
 143 expressed and are present on the order of $\sim 10^4$ per cell, which exceeds the generic estimate given
 144 in **Figure 2(A)**. Together, this generic estimation and the specific examples of induced expression
 145 suggest that transport of carbon across the cell membrane, while critical for growth, is not the
 146 rate-limiting step of cell division.

147 In the context of speeding up growth, one additional limitation is the fact that the cell's inner
 148 membrane is occupied by a multitude of other membrane proteins. Considering a rule-of-thumb
 149 for the surface area of *E. coli* of about $6 \mu\text{m}^2$ (BNID: 101792, **Milo et al. (2010)**), we expect an
 150 areal density for 1,000 transporters to be approximately 200 transporters/ μm^2 . For a glucose
 151 transporter occupying about $50 \text{ nm}^2/\text{dimer}$, this amounts to about only 1 percent of the total inner
 152 membrane (**Szenk et al.**, 2017). In addition, bacterial cell membranes typically have densities of
 153 10^5 proteins/ μm^2 (**Phillips, 2018**), implying that the cell could accommodate more transporters if it
 154 were rate limiting.

155 Phosphorus and Sulfur Transport

156 We now turn our attention towards other essential elements, namely phosphorus and sulfur.
 157 Phosphorus is critical to the cellular energy economy in the form of high-energy phosphodiester
 158 bonds making up DNA, RNA, and the NTP energy pool as well as playing a critical role in the post-
 159 translational modification of proteins and defining the polar-heads of lipids. In total, phosphorus
 160 makes up $\approx 3\%$ of the cellular dry mass which in typical experimental conditions is in the form of
 161 inorganic phosphate. The cell membrane has remarkably low permeability to this highly-charged
 162 and critical molecule, therefore requiring the expression of active transport systems. In *E. coli*, the
 163 proton electrochemical gradient across the inner membrane is leveraged to transport inorganic
 164 phosphate into the cell (**Rosenberg et al.**, 1977). Proton-solute symporters are widespread in *E. coli*
 165 (**Ramos and Kaback, 1977; Booth et al., 1979**) and can have rapid transport rates of 50 molecules
 166 per second for sugars and other solutes (BNID: 103159; 111777, **Milo et al. (2010)**). In *E. coli* the PitA
 167 phosphate transport system has been shown to very tightly coupled with the proton electrochemical

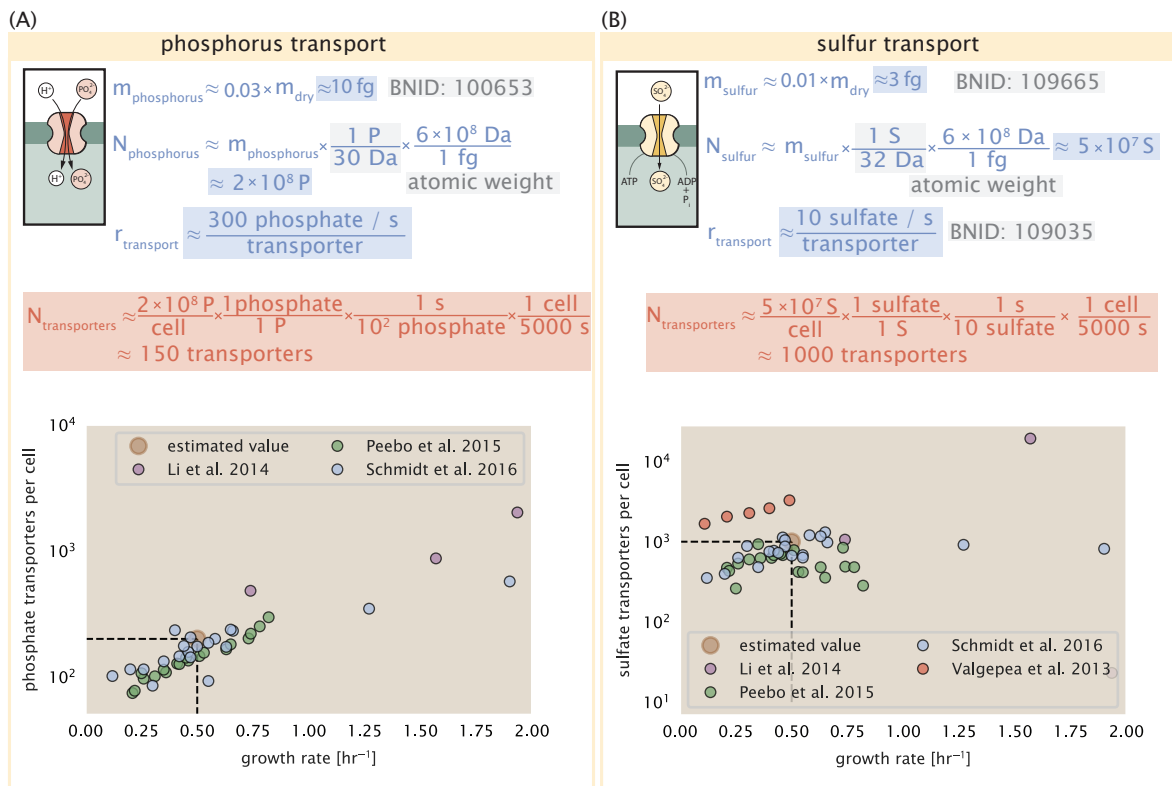


Figure 3. Estimates and measurements of phosphate and sulfate transport systems as a function of growth rate. (A) Estimate for the number of PitA phosphate transport systems needed to maintain a 3% phosphorus *E. coli* dry mass. Points in plot correspond to the total number of PitA transporters per cell. (B) Estimate of the number of CysUWA complexes necessary to maintain a 1% sulfur *E. coli* dry mass. Points in plot correspond to average number of CysUWA transporter complexes that can be formed given the transporter stoichiometry [CysA]₂[CysU][CysW][Sbp/CysP].

168 gradient with a 1:1 proton:phosphate stoichiometric ratio (*Harris et al., 2001; Feist et al., 2007*).
 169 Illustrated in *Figure 3(A)*, we can estimate that ≈ 300 phosphate transporters are necessary to
 170 maintain an $\approx 3\%$ dry mass with a 6,000 s division time. This estimate is again satisfied when we
 171 examine the observed copy numbers of PitA in proteomic data sets (plot in *Figure 3(A)*). While our
 172 estimate is very much in line with the observed numbers, we emphasize that this is likely a slight
 173 over estimate of the number of transporters needed as there are other phosphorous scavenging
 174 systems, such as the ATP-dependent phosphate transporter Pst system which we have neglected.
 175 Satisfied that there are a sufficient number of phosphate transporters present in the cell, we
 176 now turn to sulfur transport as another potentially rate limiting process. Similar to phosphate,
 177 sulfate is highly-charged and not particularly membrane permeable, requiring active transport.
 178 While there exists a H⁺/sulfate symporter in *E. coli*, it is in relatively low abundance and is not well
 179 characterized (*Zhang et al., 2014a*). Sulfate is predominantly acquired via the ATP-dependent ABC
 180 transporter CysUWA system which also plays an important role in selenium transport (*Sekowska
 181 et al., 2000; Sirko et al., 1995*). While specific kinetic details of this transport system are not readily
 182 available, generic ATP transport systems in prokaryotes transport on the order of 1 to 10 molecules
 183 per second (BNID: 109035, *Milo et al. (2010)*). Combining this generic transport rate, measurement
 184 of sulfur comprising 1% of dry mass, and a 6,000 second division time yields an estimate of \approx
 185 1000 CysUWA complexes per cell (*Figure 3(B)*). Once again, this estimate is in notable agreement
 186 with proteomic data sets, suggesting that there are sufficient transporters present to acquire the
 187 necessary sulfur. In a similar spirit of our estimate of phosphorus transport, we emphasize that
 188 this is likely an overestimate of the number of necessary transporters as we have neglected other
 189 sulfur scavenging systems that are in lower abundance.

190 **Nitrogen Transport**

191 Finally, we turn to nitrogen transport as the last remaining transport system highlighted in **Figure 1**.
 192 Unlike phosphate, sulfate, and various sugar molecules, nitrogen in the form of ammonia can readily
 193 diffuse across the cell membrane and has a permeability on par with water ($\approx 10^5$ nm/s, BNID:110824
 194 *Milo et al. (2010)*). In particularly nitrogen-poor conditions, *E. coli* expresses a transporter (AmtB)
 195 which appears to aid in nitrogen assimilation, though the mechanism and kinetic details of transport
 196 is still a matter of debate (*van Heeswijk et al., 2013; Khademi et al., 2004*). Beyond ammonia,
 197 another plentiful source of nitrogen come in the form of glutamate, which has its own complex
 198 metabolism and scavenging pathways. However, nitrogen is plentiful in the growth conditions
 199 examined in this work, permitting us to neglect nitrogen transport as a potential rate limiting
 200 process in cell division.

201 **Function of the Central Dogma**

202 Up to this point, we have considered a variety of transport and biosynthetic processes that are
 203 critical to acquiring and generating new cell mass. While there are of course many other metabolic
 204 processes we could consider and perform estimates of (such as the components of fermentative
 205 versus aerobic respiration), we now turn our focus to some of the most central processes which
 206 must be undertaken irrespective of the growth conditions – the processes of the central dogma.

207 **DNA**

208 Most bacteria (including *E. coli*) harbor a single, circular chromosome and can have extra-chromosomal
 209 plasmids up to ~ 100 kbp in length. We will focus our quantitative thinking solely on the chromo-
 210 some of *E. coli* which harbors ≈ 5000 genes and $\approx 5 \times 10^6$ base pairs. To successfully divide and
 211 produce viable progeny, this chromosome must be faithfully replicated and segregated into each
 212 nascent cell. We again rely on the near century of literature in molecular biology to provide some
 213 insight on the rates and mechanics of the replicative feat as well as the production of the required
 214 starting materials, dNTPs.

215 **dNTP synthesis**

216 We begin our exploration DNA replication by examining the production of the deoxyribonucleotide
 217 triphosphates (dNTPs). The four major dNTPs (dATP, dTTP, dCTP, and dGTP) are synthesized *de novo*
 218 in separate pathways, requiring different building blocks. However, a critical step present in all
 219 dNTP synthesis pathways is the conversion from ribonucleotide to deoxyribonucleotide via the
 220 removal of the 3' hydroxyl group of the ribose ring (*Rudd et al., 2016*). This reaction is mediated by a
 221 class of enzymes termed ribonucleotide reductases, of which *E. coli* possesses two aerobically active
 222 complexes (termed I and II) and a single anaerobically active enzyme. Due to their peculiar formation
 223 of a radical intermediate, these enzymes have received much biochemical, kinetic, and structural
 224 characterization. One such work (*Ge et al., 2003*) performed a detailed *in vitro* measurement of the
 225 steady-state kinetic rates of these complexes, revealing a turnover rate of ≈ 10 dNTP per second.

226 Since this reaction is central to the synthesis of all dNTPs, it is reasonable to consider the
 227 abundance of these complexes is a measure of the total dNTP production in *E. coli*. Illustrated
 228 schematically in **Figure 4** (A), we consider the fact that to replicate the cell's genome, on the order of
 229 $\approx 10^7$ dNTPs must be synthesized. Assuming a production rate of 10 per second per ribonucleotide
 230 reductase complex and a cell division time of 6000 seconds, we arrive at an estimate of ≈ 150
 231 complexes needed per cell. As shown in the bottom panel of **Figure 4** (A), this estimate agrees
 232 with the experimental measurements of these complexes abundances within $\approx 1/2$ an order of
 233 magnitude.

234 Recent work has revealed that during replication, the ribonucleotide reductase complexes
 235 coalesce to form discrete foci colocalized with the DNA replisome complex (*Sánchez-Romero et al.,*
 236 *2011*). This is particularly pronounced in conditions where growth is slow, indicating that spatial
 237 organization and regulation of the activity of the complexes plays an important role.

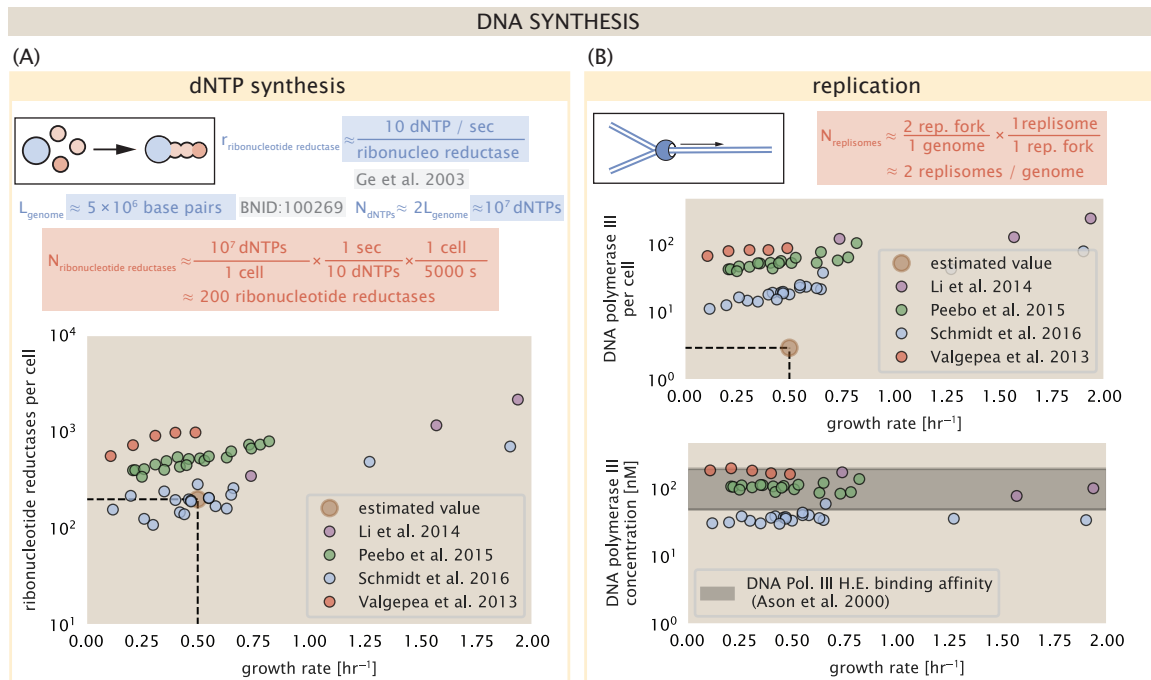


Figure 4. Complex abundance estimates for dNTP synthesis and DNA replication. (A) Estimate of the number of ribonucleotide reductase enzymes needed to facilitate the synthesis of $\approx 10^7$ dNTPs over the course of a 6000 second generation time. Points in the plot correspond to the total number of ribonucleotide reductase I ($[NrdA]_2[NrdB]_2$) and ribonucleotide reductase II ($[NrdE]_2[NrdF]_2$) complexes. (B) An estimate for the minimum number of DNA polymerase holoenzyme complexes needed to facilitate replication of a single genome. Points in the top plot correspond to the total number of DNA polymerase III holoenzyme complexes ($[DnaE]_3[DnaQ]_3[HolE]_3[DnaX]_5[HolB][HolA][DnaN]_4[HolC]_4[HolD]_4$) per cell. Bottom plot shows the effective concentration of DNA polymerase III holoenzyme given cell volumes calculated from the growth rate as in *Si et al. (2019)* (See Appendix Section 4).

238 DNA Replication

239 We now turn our focus to the integration of these dNTP building blocks into the replicated chromo-
 240 some strand via the DNA polymerase. Replication is initiated at a single region of the chromosome
 241 termed the *oriC* locus at which a pair of DNA polymerases bind and begin their high-fidelity replica-
 242 tion of the genome in opposite directions. Assuming equivalence between the two replication forks,
 243 this means that the two DNA polymerase complexes (termed replisomes) meet at the midway point
 244 of the circular chromosome termed the *ter* locus. The kinetics of the five types of DNA polymerases
 245 (I – V) have been intensely studied, revealing that DNA polymerase III performs the high fidelity
 246 processive replication of the genome with the other "accessory" polymerases playing auxiliary roles
 247 (*Fijalkowska et al., 2012*). *In vitro* measurements have shown that DNA Polymerase III copies DNA
 248 at a rate of \approx 600 nucleotides per second (BNID: 104120, *Milo et al. (2010)*). Therefore, to replicate a
 249 single chromosome, two DNA polymerases replicating at their maximal rate would copy their entire
 250 genome in \approx 4000 s. Thus, with a division time of 5000 s (our "typical" growth rate for the purposes
 251 of this work), there is sufficient time for a pair of DNA polymerase III complexes to replicate the
 252 entire genome. However, this estimate implies that 4000 s would be the upper-limit time scale for
 253 bacterial division which is at odds with the familiar 20 minute (1200 s) doubling time of *E. coli* in rich
 254 medium.

255 It is well known that *E. coli* can parallelize its DNA replication such that multiple chromosomes
 256 are being replicated at once, with as many as 10 - 12 replication forks at a given time (*Bremer*
and Dennis, 2008; Si et al., 2017). Thus, even in rapidly growing cultures, we expect only a few
 257 polymerases (\approx 10) are needed to replicate the chromosome per cell doubling. However, as shown
 258 in **Figure 4(B)**, DNA polymerase III is nearly an order of magnitude more abundant. This
 259 discrepancy can be understood by considering its binding constant to DNA. DNA polymerase III
 260 is highly processive, facilitated by a strong affinity of the complex to the DNA. *In vitro* biochemical
 261 characterization has quantified the K_D of DNA polymerase III holoenzyme to single-stranded and
 262 double-stranded DNA to be 50 and 200 nM, respectively (*Ason et al., 2000*). The bottom plot in
 263 **Figure 4** (B) shows that the concentration of the DNA polymerase III across all data sets and growth
 264 conditions is within this range. Thus, while the copy number of the DNA polymerase III is in excess
 265 of the strict number required to replicate the genome, its copy number appears to vary such that its
 266 concentration is approximately equal to the dissociation constant to the DNA. While the processes
 267 regulating the initiation of DNA replication are complex and involve more than just the holoenzyme,
 268 these data indicate that the kinetics of replication rather than the explicit copy number of the DNA
 269 polymerase III holoenzyme is the more relevant feature of DNA replication to consider. In light
 270 of this, the data in **Figure 4(B)** suggests that for bacteria like *E. coli*, DNA replication does not represent a rate-limiting step in cell division. However, it is worth noting that for bacterium like *C. crescentus* whose chromosomal replication is initiated only once per cell cycle (*Jensen et al., 2001*), the time to double their chromosome likely represents an upper limit to their growth rate.

275 RNA Synthesis

276 With the machinery governing the replication of the genome accounted for, we now turn our
 277 attention to the next stage of the central dogma – the transcription of DNA to form RNA. We
 278 primarily consider three major groupings of RNA, namely the RNA associated with ribosomes
 279 (rRNA), the RNA encoding the amino-acid sequence of proteins (mRNA), and the RNA which links
 280 codon sequence to amino-acid identity during translation (tRNA). Despite the varied function of
 281 these RNA species, they share a commonality in that they are transcribed from DNA via the action
 282 of RNA polymerase. In the coming paragraphs, we will consider the synthesis of RNA as a rate
 283 limiting step in bacterial division by estimating how many RNA polymerases must be present to
 284 synthesize all necessary rRNA, mRNA, and tRNA.

285 rRNA

286 We begin with an estimation of the number of RNA polymerases needed to synthesize the rRNA
 287 that serve as catalytic and structural elements of the ribosome. Each ribosome contains three rRNA
 288 molecules of lengths 120, 1542, and 2904 nucleotides (BNID: 108093, *Milo et al. (2010)*), meaning
 289 each ribosome contains \approx 4500 nucleotides. As the *E. coli* RNA polymerase transcribes DNA to RNA
 290 at a rate of \approx 40 nucleotides per second (BNID: 101904, *Milo et al. (2010)*), it takes a single RNA
 291 polymerase \approx 100 s to synthesize the RNA needed to form a single functional ribosome. Therefore,
 292 in a 5000 s division time, a single RNA polymerase transcribing rRNA at a time would result in only
 293 \approx 50 functional ribosomal rRNA units – far below the observed number of \approx 10^4 ribosomes per cell.

294 Of course, there can be more than one RNA polymerase transcribing the rRNA genes at any
 295 given time. To elucidate the *maximum* number of rRNA units that can be synthesized given a single
 296 copy of each rRNA gene, we will consider a hypothesis in which the rRNA operon is completely tiled
 297 with RNA polymerase. *In vivo* measurements of the kinetics of rRNA transcription have revealed that
 298 RNA polymerases are loaded onto the promoter of an rRNA gene at a rate of \approx 1 per second (BNID:
 299 111997; 102362, *Milo et al. (2010)*). If RNA polymerases are being constantly loaded on to the rRNA
 300 genes at this rate, then we can assume that \approx 1 functional rRNA unit is synthesized per second.
 301 With a 5000 second division time, this hypothesis leads to a maximal value of 5000 functional rRNA
 302 units, still undershooting the observed number of 10^4 ribosomes per cell.

303 *E. coli* has evolved a clever mechanism to surpass this kinetic limit for the rate of rRNA production.
 304 Rather than having only one copy of each rRNA gene, *E. coli* has seven copies of the operon
 305 (BIND: 100352, *Milo et al. (2010)*) four of which are localized directly adjacent to the origin of
 306 replication (*Birnbaum and Kaplan, 1971*). As fast growth also implies an increased gene dosage due
 307 to parallelized chromosomal replication, the total number of rRNA genes can be on the order of \approx
 308 10 – 70 copies at moderate to fast growth rates (*Stevenson and Schmidt, 2004*). Using our standard
 309 time scale of a 5000 second division time, we can make the lower-bound estimate that the typical
 310 cell will have 7 copies of the rRNA operon. Synthesizing one functional rRNA unit per second per
 311 rRNA operon, a total of 4×10^4 rRNA units can be synthesized, comfortably above the observed
 312 number of ribosomes per cell.

313 How many RNA polymerases are then needed to constantly transcribe 7 copies of the rRNA
 314 genes? We approach this estimate by considering the maximum number of RNA polymerases tiled
 315 along the rRNA genes with a loading rate of 1 per second and a transcription rate of 40 nucleotides
 316 per second. Considering that a RNA polymerase has a physical footprint of approximately 40
 317 nucleotides (BNID: 107873, *Milo et al. (2010)*), we can expect \approx 1 RNA polymerase per 80 nucleotides.
 318 With a total length of \approx 4500 nucleotides per operon and 7 operons per cell, the maximum number
 319 of RNA polymerases that can be transcribing rRNA at any given time is \approx 400. As we will see in the
 320 coming sections, the synthesis of rRNA is the dominant requirement of the RNA polymerase pool.

321 mRNA

322 To form a functional protein, all protein coding genes must first be transcribed from DNA to form
 323 an mRNA molecule. While each protein requires an mRNA blueprint, many copies of the protein
 324 can be synthesized from a single mRNA. Factors such as strength of the ribosomal binding site,
 325 mRNA stability, and rare codon usage frequency dictate the number of proteins that can be made
 326 from a single mRNA, with yields ranging from 10^1 to 10^4 (BNID: 104186; 100196; 106254, *Milo et al.*
 327 (*2010*)). Computing the geometric mean of this range yields \approx 1000 proteins synthesized per mRNA,
 328 a value that agrees with experimental measurements of the number of proteins per cell ($\approx 3 \times 10^6$,
 329 BNID: 100088, *Milo et al. (2010)*) and total number of mRNA per cell ($\approx 3 \times 10^3$, BNID: 100064, *Milo*
 330 *et al. (2010)*).

331 This estimation captures the *steady-state* mRNA copy number, meaning that at any given time,
 332 there will exist approximately 3000 unique mRNA molecules. To determine the *total* number of
 333 mRNA that need to be synthesized over the cell's lifetime, we must consider degradation of the
 334 mRNA. In most bacteria, mRNAs are rather unstable with life times on the order of several minutes

(BNID: 104324; 106253; 111927; 111998, *Milo et al. (2010)*). For convenience, we assume that the typical mRNA in our cell of interest has a typical lifetime of \approx 300 seconds. Using this value, we can determine the total mRNA production rate to maintain a steady-state copy number of 3000 mRNA per cell. While we direct the reader to the appendix for a more detailed discussion of mRNA transcriptional dynamics, we state here that the total mRNA production rate must be on the order of \approx 15 mRNA per second. In *E. coli*, the average protein is \approx 300 amino acids in length (BNID: 108986; *Milo et al. (2010)*), meaning that the corresponding mRNA is \approx 900 nucleotides which we will further approximate as \approx 1000 nucleotides to account for the non-protein coding regions on the 5' and 3' ends. This means that the cell must have enough RNA polymerase molecules about to sustain a transcription rate of $\approx 1.5 \times 10^4$ nucleotides per second. Knowing that a single RNA polymerase polymerizes RNA at a clip of 40 nucleotides per second, we arrive at a comfortable estimate of \approx 250 RNA polymerase complexes needed to satisfy the mRNA demands of the cell. It is worth noting that this number is approximately half of that required to synthesize enough rRNA, as we saw in the previous section. We find this to be a striking result as these 250 RNA polymerase molecules are responsible for the transcription of the \approx 4000 protein coding genes that are not ribosome associated.

351 tRNA

352 The final class of RNA molecules worthy of quantitative consideration is the pool of tRNAs used during translation to map codon sequence to amino acid identity. Unlike mRNA or rRNA, each individual tRNA is remarkably short, ranging from 70 to 95 nucleotides each (BNID: 109645; 353 102340, *Milo et al. (2010)*). What they lack in length, they make up for in abundance. There are 354 approximately \approx 3000 tRNA molecules present for each of the 20 amino acids (BNID: 105280, *Milo et al. (2010)*), although the precise copy number is dependent on the identity of the ligated amino 355 acid. Using these values, we make the estimate that $\approx 5 \times 10^6$ nucleotides are sequestered in tRNA 356 per cell. Unlike mRNA, tRNA is remarkably stable with typical lifetimes *in vivo* on the order of \approx 48 357 hours (*Abelson et al., 1974; Svenningsen et al., 2017*) – well beyond the timescale of division. Once 358 again using our rule-of-thumb for the rate of transcription to be 40 nucleotides per second and 359 assuming a division time of \approx 5000 seconds, we arrive at an estimate of \approx 20 RNA polymerases 360 to synthesize enough tRNA. This requirement pales in comparison to the number of polymerases 361 needed to generate the rRNA and mRNA pools and can be neglected as a significant transcriptional 362 burden.

366 RNA Polymerase and σ -factor Abundance

367 These estimates, summarized in *Figure 5 (A)*, reveal that synthesis of rRNA and mRNA are the dominant 368 RNA species synthesized by RNA polymerase, suggesting the need for \approx 700 RNA polymerases 369 per cell. As is revealed in *Figure 5 (B)*, this estimate is about an order of magnitude below the observed 370 number of RNA polymerase complexes per cell (\approx 5000 - 7000). The disagreement between the estimated 371 number of RNA polymerases and these observations are at least consistent with recent literature 372 revealing that \approx 80 % of RNA polymerases in *E. coli* are not transcriptionally active 373 (*Patrick et al., 2015*). Our estimate ignores the possibility that some fraction is only nonspecifically 374 bound to DNA, as well as the obstacles that RNA polymerase and DNA polymerase present for each 375 other as they move along the DNA (*Finkelstein and Greene, 2013*).

376 In addition, it is also vital to consider the role of σ -factors which help RNA polymerase identify 377 and bind to transcriptional start sites (*Browning and Busby, 2016*). Here we consider σ^{70} (RpoD) 378 which is the dominant "general-purpose" σ -factor in *E. coli*. While initially thought of as being solely 379 involved in transcriptional initiation, the past two decades of single-molecule work has revealed 380 a more multipurpose role for σ^{70} including facilitating transcriptional elongation (*Kapanidis et al., 2005; Goldman et al., 2015; Perdue and Roberts, 2011; Mooney and Landick, 2003; Mooney et al., 2005*). *Figure 5 (B)* is suggestive of such a role as the number of σ^{70} proteins per cell is in close 381 agreement with our estimate of the number of transcriptional complexes needed.

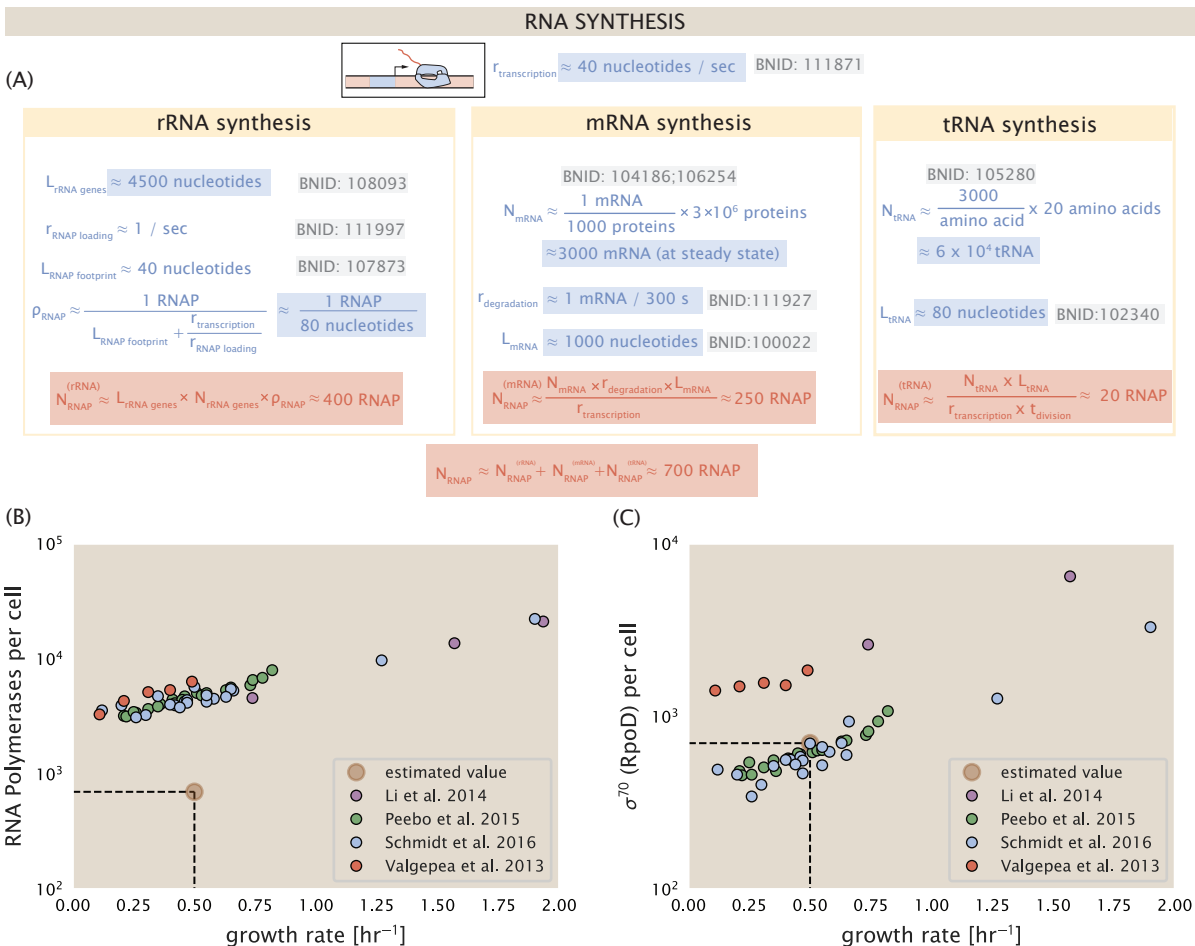


Figure 5. Estimation of the RNA polymerase demand and comparison with experimental data. (A) Estimations for the number of RNA polymerase needed to synthesize sufficient quantities of rRNA, mRNA, and tRNA from left to right, respectively. Bionumber Identifiers (BNIDs) are provided for key quantities used in the estimates. (B) The RNA polymerase core enzyme copy number as a function of growth rate. Colored points correspond to the average number RNA polymerase core enzymes that could be formed given a subunit stoichiometry of $[RpoA]_2[RpoC][RpoB]$. (C) The abundance of σ^{70} as a function of growth rate. Estimated value for the number of RNAP is shown in (B) and (C) as a translucent brown point at a growth rate of 0.5 hr^{-1} .

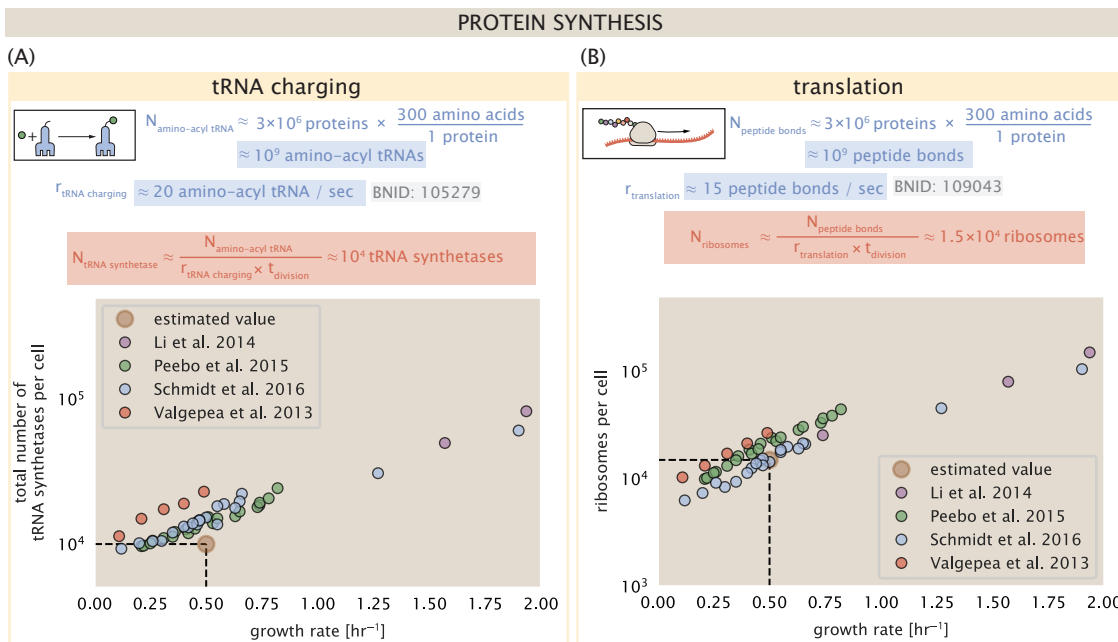


Figure 6. Estimation of the required tRNA synthetases and ribosomes. (A) Estimation for the number of tRNA synthetases that will supply the required amino acid demand. The sum of all tRNA synthetases copy numbers are plotted as a function of growth rate ([ArgS], [CysS], [GlnS], [GlxS], [IleS], [LeuS], [ValS], [AlaS]₂, [AsnS]₂, [AspS]₂, [TyrS]₂, [TrpS]₂, [ThrS]₂, [SerS]₂, [ProS]₂, [PheS]₂[PheT]₂, [MetG]₂, [lysS]₂, [HisS]₂, [GlyS]₂[GlyQ]₂). (B) Estimation for the number of ribosomes required to synthesize all proteins in the cell. The average abundance of ribosomes is plotted as a function of growth rate. Our estimated values are shown for a growth rate of 0.5 hr⁻¹.

384 While these estimates and comparison with experimental data reveal an interesting dynamic at
 385 play between the transcriptional demand and copy numbers of the corresponding machinery, these
 386 findings illustrate that transcription cannot be the rate limiting step in bacterial division. **Figure 5**
 387 (A) reveals that the availability of RNA polymerase is not a limiting factor for cell division as the cell
 388 always has an apparent ~10-fold excess than needed. Furthermore, if more transcriptional activity
 389 was needed to satisfy the cellular requirements, more σ^{70} -factors could be expressed to utilize a
 390 larger fraction of the RNA polymerase pool.

391 Protein synthesis

392 Lastly, we turn our attention to the process of translation. So far in our estimates there have been
 393 little to suggest any apparent limit on the cell's ability to produce the required number protein
 394 species. Even in our example of *E. coli* grown under different carbohydrate sources (**Figure 2(B)**), cells
 395 are able to utilize alternative carbon sources by inducing the expression of additional membrane
 396 transporters and enzymes. For a doubling time of 5000 seconds, *E. coli* has roughly 3×10^6 proteins
 397 per cell, which for an average protein of 300 aa, amounts to $\approx 10^9$ peptide bonds that must be
 398 formed. This also corresponds to the number of amino-acyl tRNA that are used, with the pool of
 399 tRNA continuously recharged with new amino acids by tRNA synthetases. At a rate of charging of
 400 about 20 amino-acyl tRNA per second (BNID: 105279, **Milo et al. (2010)**), we find that cells have
 401 more than sufficient tRNA synthetases to meet the demand of ribosomes during protein synthesis
 402 (**Figure 6(A)**).

403 If we consider an elongation rate of ≈ 15 peptide bonds per second (BNID: 114271, **Milo et al.**
 404 **(2010); Dai et al. (2016)**), the formation of $\approx 10^9$ peptide bonds would require 1.5×10^4 ribosomes at
 405 a growth rate of 0.5 hr^{-1} . This is indeed consistent with the experimental data shown in **Figure 6(B)**.
 406 However, in view of our earlier estimate on rRNA, which suggest that rRNA operons need to be
 407 nearly packed with transcribing RNA polymerase even at relatively slow growth, there is a possibility
 408 that ribosomes might limit growth. While the transcriptional demand for ribosomal proteins will

409 not be nearly as high as rRNA genes, other ribosomal proteins like the translation elongation
 410 factor EF-Tu is the most highly expressed protein and is present in two copies on the chromosome.
 411 Experimentally, consecutive deletion of rRNA operons showed a significant reduction in growth rate
 412 in rich media when cells had only 3 or less (*Levin et al., 2017*).

413 We can begin to gain some intuition into how translation, or ribosomes more specifically, might
 414 limit growth by noting that the total number of peptide bonds generated as the cell doubles, N_{aa} ,
 415 which we used in our calculation above, will be given by, $\tau \cdot r_t \cdot R$. Here, τ refers to the doubling time
 416 of the cell under steady-state growth, r_t is the maximum translation elongation rate, and R is the
 417 average number of ribosomes per cell. With the growth rate related to the cell doubling time by
 418 $\lambda = \ln(2)/\tau$, we can write the translation-limited growth rate as,

$$\lambda_{\text{translation-limited}} = \frac{\ln(2) \cdot r_t \cdot R}{N_{aa}}. \quad (1)$$

419 Alternatively, since N_{aa} is related to the total protein mass through the molecular weight of each
 420 protein, we can also consider the growth rate in terms of ribosomal mass fraction. By making the
 421 approximation that an average amino acid has a molecular weight of 110 Da (see *Figure 7(A)*), we
 422 can rewrite the growth rate as,

$$\lambda_{\text{translation-limited}} \approx \frac{\ln(2) \cdot r_t}{L_R} \Phi_R, \quad (2)$$

423 where L_R is the total length in amino acids that make up a ribosome, and Φ_R is the ribosomal
 424 mass fraction. This is plotted as a function of ribosomal fraction Φ_R in *Figure 7(A)*, where we take
 425 $L_R \approx 7459$ aa, corresponding to the length in amino acids for all ribosomal subunits of the 50S and
 426 30S complex. This formulation assumes that the cell can also transcribe the required amount of
 427 rRNA, allowing us to consider the inherent limit on growth set by the ribosome.

428 Perhaps the first thing to notice is that there is a maximum growth rate at about $\lambda \approx 6\text{hr}^{-1}$, or
 429 doubling time of about 7 minutes (dashed line). This growth rate can be viewed as an inherent
 430 maximum rate due to the need for the cell to double the cell's entire ribosomal mass. Interestingly,
 431 this limit is independent of the absolute number of ribosomes, but rather is simply given by
 432 time to translate an entire ribosome, L_R/r_t . As shown in *Figure 7(B)*, we can reconcile this with
 433 the observation that in order to double the average number of ribosomes, each ribosome must
 434 produce a second ribosome. This is a process that cannot be parallelized.

435 For reasonable values of Φ_R , in the range of about 0.1 - 0.3 (*Scott et al., 2010*), the maximum
 436 growth rate is in line with experimentally reported growth rates around 0.5 - 2 hr^{-1} . Here we have
 437 implicitly assumed that translation proceeds randomly, without preference between ribosomal or
 438 non-ribosomal mRNA, which appears reasonable. Importantly, in order for a cell to scale this limit
 439 set by Φ_R the cell must increase its ribosomal abundance, either by synthesizing more ribosomes
 440 or reducing the fraction of non-ribosomal proteins.

441 While it is common for bacteria to decrease their ribosomal abundance in poorer nutrient
 442 conditions (*Scott et al. (2010); Lieberman et al. (2014)*), this does not decrease to zero. From
 443 the perspective of a bacterium dealing with uncertain nutrient conditions, there is likely a benefit
 444 for the cell to maintain some relative fraction of ribosomes to support rapid growth as nutrient
 445 conditions improve. However, if we consider a scenario where nutrient conditions become poorer
 446 and poorer, there will be a regime where ribosomes are in excess of the nutrient supply. If the cell
 447 is to maintain steady-state growth, it will need to attenuate its translational activity since ribosomes
 448 would otherwise exhaust their supply of amino acids and bring cell growth to a halt (*Figure 7(C)*). In
 449 the next section we will consider this more specifically for *E. coli*, which has been shown to maintain
 450 a relatively high elongation rate even in stationary phase (≈ 8 aa/s, *Dai et al. (2016)*) where cell
 451 growth is minimal.

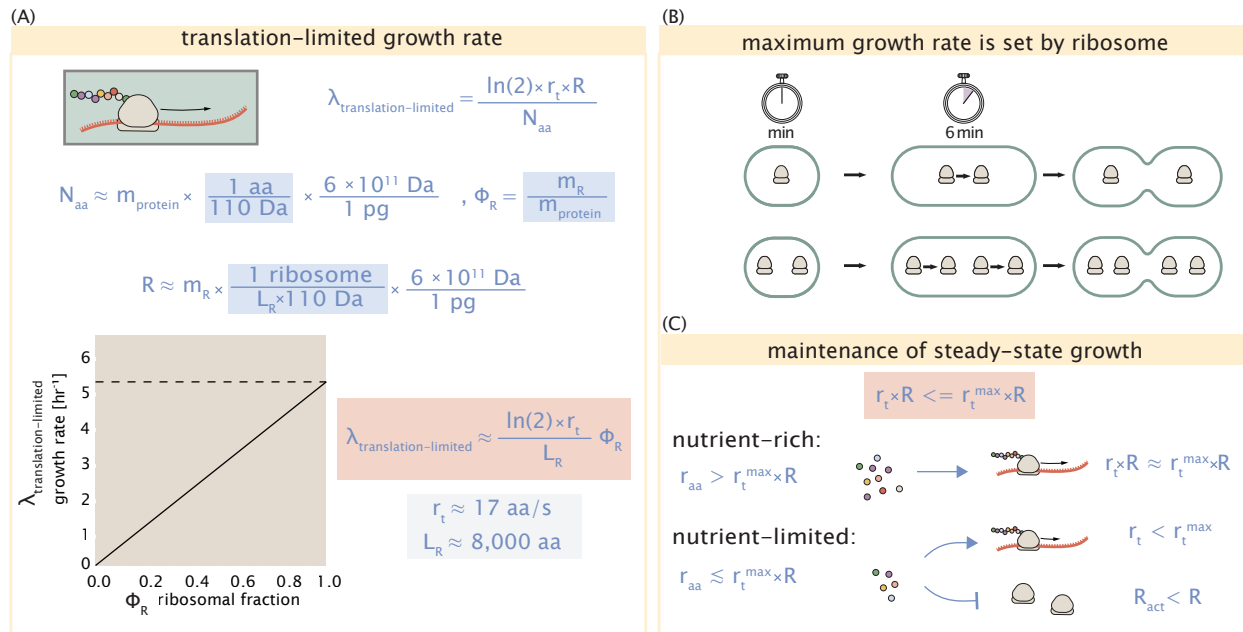


Figure 7. Translation-limited growth rate. (A) Here we consider the translation-limited growth as a function of ribosomal fraction. By mass balance, the time required to double the entire proteome (N_{aa} / r_t) sets the translation-limited growth rate, $\lambda_{\text{translation-limited}}$. Here N_{aa} is effectively the number of peptide bonds that must be translated, r_t is the translation elongation rate, and R is the number of ribosomes. This can also be re-written in terms of the ribosomal mass fraction $\Phi_R = m_R / m_{\text{protein}}$, where m_R is the total ribosomal mass and m_{protein} is the mass of all proteins in the cell. L_R refers to the summed length of the ribosome in amino acids. $\lambda_{\text{translation-limited}}$ is plotted as a function of Φ_R (solid line). (B) The dashed line in part (A) identifies a maximum growth rate that is set by the ribosome. Specifically, this growth rate corresponds to the time required to translate an entire ribosome, L_R / r_t . This is a result that is independent of the number of ribosomes in the cell as shown schematically here. (C) Schematic showing translation-specific requirements for maintenance of steady-state growth. In a nutrient rich environment, amino acid supply r_{aa} is sufficiently in excess of demand by ribosomes translating at their maximal rate. In poorer nutrient conditions, reduced amino acid supply r_{aa} will decrease the rate of elongation. In a regime where r_{aa} is less than $r_t \cdot R$, the number of actively translating ribosomes will need to be reduced in order to maintain steady-state growth.

452 **Multiple replication forks bias ribosome abundance.**

453 *E. coli* cells grow by an adder mechanism, whereby cells add a constant volume with each cell
 454 division (*Taheri-Araghi et al., 2015*). In conjunction with this, additional rounds of DNA replication
 455 are triggered when cells reach a critical volume per origin of replication (*Figure 8(A)*). This leads to
 456 the classically-described exponential increase in cell size with growth rate *Schaechter et al. (1958)*;
 457 *Si et al. (2017, 2019)*. In the context of maximizing growth rate, it is notable that the majority of
 458 ribosomal proteins and rRNA operons are found closer to the DNA origin. Given the necessity of
 459 increasing the effective number of rRNA operons at faster growth rates, this raises the possibility
 460 that the observed size scaling and increase in chromosomal equivalents might simply be as a means
 461 for the cell to tune biosynthetic rates according to its physiological state.

462 While an increase in transcription has been observed for genes near the origin in rapidly growing
 463 *E. coli* (*Scholz et al., 2019*), we were unaware of such characterization at the proteomic level. In order
 464 to test whether such a skew in expression exists at the protein level at faster growth, we calculated
 465 a running boxcar average of protein copy number as a function of their transcriptional start sites.
 466 While absolute protein copy numbers vary substantially across the chromosome, we indeed observe
 467 a bias in expression under faster growth conditions (*Figure 8(B)*, showing the result using a 0.5 kb
 468 averaging window). The dramatic change in protein copy number near the origin mainly reflects
 469 the increase in ribosomal protein expression. This trend is in contrast to slower growth conditions
 470 where the average copy number is more uniform across the length of the chromosome.

471 If ribosomal genes (rRNA and ribosomal proteins) are being synthesized according to their
 472 available gene dosage we can make two related hypotheses about how ribosomal abundance
 473 should vary with chromosomal content. The first is that the ribosomal protein fraction should
 474 increase in proportion to the average ratio of DNA origins to DNA termini ($\langle \# \text{ ori} \rangle / \langle \# \text{ ter} \rangle$ ratio),
 475 which is a consequence of the skew in DNA dosage as cells grow faster. The second is that the
 476 absolute number of ribosomes should increase in proportion to the number of DNA origins ($\langle \# \text{ ori} \rangle$), since this will reflect the total gene dosage at a particular growth condition.

477 In order to test these hypotheses we considered the experimental data from *Si et al. (2017)*,
 478 which determined these parameters under nutrient-limited growth. $\langle \# \text{ ori} \rangle / \langle \# \text{ ter} \rangle$ ratio depends
 479 on how quickly chromosomes are replicated relative the cell's doubling time τ and is given by $2^{\tau_C/\tau}$.
 480 Here τ_C is the time taken to replicate the chromosome, referred to as the C period of cell division.
 481 In *Figure 8(C)* we plot τ_C versus τ that were measured, with data points in red corresponding to *E. coli*
 482 strain MG1655, and blue to strain NCM3722. In their work they also measured the total RNA to
 483 protein ratio which reflects ribosomal abundance and we show that data along with other recent
 484 measurements from *Dai et al.* Indeed we find that the ribosomal fraction increases with $\langle \# \text{ ori} \rangle$
 485 / $\langle \# \text{ ter} \rangle$ (*Figure 8(C)*). Across our different proteomic data sets there also appeared two distinct
 486 trends. To consider the possibility that this may reflect systematic differences in how the data
 487 was generated, we also considered recent measurements of total RNA to protein ratio across the
 488 growth rates considered, which provide an alternative measure of ribosomal abundance (RNA to
 489 protein ratio $\approx \Phi_R \times 2.1$ *Dai et al. (2016)*). While these showed a similar correlation, they were most
 490 consistent with the proteomic data from *Schmidt et al. (2016)* and *Li et al. (2014)*.

491 We can similarly estimate $\langle \# \text{ ori} \rangle$, which depends on how often replication forks are initiated
 492 per cell cycle. This is given by the number of overlapping cell cycles, $2^{\tau_{\text{cyc}}/\tau}$, where τ_{cyc} refers to
 493 the total time of chromosome replication and cell division. *Figure 8(E)* shows the associated data
 494 from *Si et al.*, which we use to estimate $\langle \# \text{ ori} \rangle$ for each growth condition of the proteomic data. In
 495 agreement with our expectations, we find a strong correlation between the ribosome copy number
 496 and estimated $\langle \# \text{ ori} \rangle$ (*Figure 8(F)*).

497 [NB: to do. 1) slow growth regime, 2) putting it all together ; cells appear to grow near the
 498 translation-limited rate ($r_i = 17 \text{ aa/s}$) across all growth conditions. Need to provide some rationalization
 499 for points above line.]

500 [NB: Titration of the cellular ppGpp concentration invoked similar proteomic changes to those

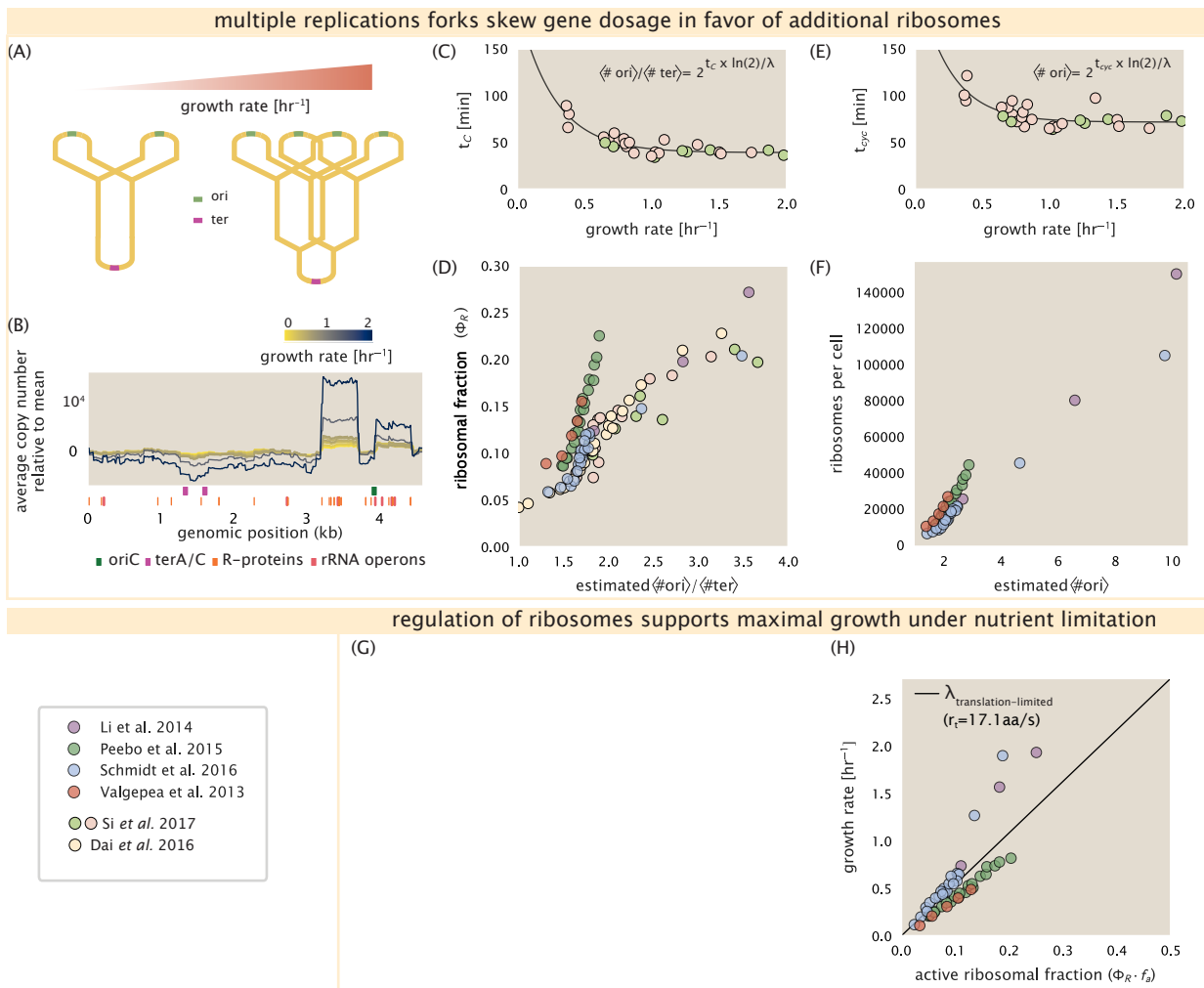


Figure 8. Multiple replication forks skew gene dosage and ribosomal content. (A) Schematic shows the expected increase in replication forks (or number of ori regions) as *E. coli* cells grow faster. (B) A running boxcar average of protein copy number is calculated for each growth condition considered by Schmidt *et al.*. A 0.5 kb averaging window was used. Protein copy numbers are reported relative to their condition-specific means in order to center all data sets. (C) and (E) show experimental data from Si *et al.* (2017). Solid lines show fits to the data, which were used to estimate $\langle \# \text{ori} \rangle / \langle \# \text{ter} \rangle$ [NB: to note fit equations]. Red data points correspond to measurements in strain MG1655, while light green points are for strain NCM3722. (D) Plot compares our estimate of $\langle \# \text{ori} \rangle / \langle \# \text{ter} \rangle$ to the experimental measurements of ribosomal abundance. Ribosomal fraction was approximated from the RNA/protein ratios of Dai *et al.* (2016) (yellow) and Si *et al.* (2017) (light red and light green) by the conversion RNA/protein ratio $\approx \Phi_R \cdot 2.1$. (F) plots the ribosome copy number estimated from the proteomic data against our estimate of $\langle \# \text{ori} \rangle$. (G) [in progress], (H) Experimental data from Dai *et al.* are used to estimate the fraction of actively translating ribosomes. The solid line represents the translation-limited growth rate for ribosomes elongating at 17.1 aa/s.

502 observed under nutrient limitation (*Zhu and Dai, 2019*). In light of our hypothesis that such changes
 503 to the proteome are intimately linked to the details of DNA replication, it was recently shown that
 504 both the $\langle \# \text{ ori} \rangle / \langle \# \text{ ter} \rangle$ and cell size lost their growth rate dependent scaling in a ppGpp null strain.
 505 Rather, cells exhibit a $\langle \# \text{ ori} \rangle / \langle \# \text{ ter} \rangle$ closer to 4 and cell size more consistent with a fast growth state
 506 (*Fernández-Coll et al., 2020*). This supports the possibility that in addition to coordinating ribosome
 507 activity, (p)ppGpp signaling may be acting to coordinate other cellular processes in accordance with
 508 nutrient conditions and biosynthetic demand. From this perspective, the increase in the rate of
 509 DNA initiation and associated increase in cell size may be viewed as a way for the cell to vary its
 510 proteomic composition and biosynthetic capacity according to its available nutrient conditions.]

511 References

- 512 Abelson, H., Johnson, L., Penman, S., and Green, H. (1974). Changes in RNA in relation to growth of the fibroblast:
 513 II. The lifetime of mRNA, rRNA, and tRNA in resting and growing cells. *Cell*, 1(4):161–165.
- 514 Aidelberg, G., Towbin, B. D., Rothschild, D., Dekel, E., Bren, A., and Alon, U. (2014). Hierarchy of non-glucose
 515 sugars in *Escherichia coli*. *BMC Systems Biology*, 8(1):133.
- 516 Antonenko, Y. N., Pohl, P., and Denisov, G. A. (1997). Permeation of ammonia across bilayer lipid membranes
 517 studied by ammonium ion selective microelectrodes. *Biophysical Journal*, 72(5):2187–2195.
- 518 Ason, B., Bertram, J. G., Hingorani, M. M., Beechem, J. M., O'Donnell, M., Goodman, M. F., and Bloom, L. B.
 519 (2000). A Model for *Escherichia coli* DNA Polymerase III Holoenzyme Assembly at Primer/Template Ends:
 520 DNA Triggers A Change In Binding Specificity of the γ Complex Clamp Loader. *Journal of Biological Chemistry*,
 521 275(4):3006–3015.
- 522 Assentoft, M., Kaptan, S., Schneider, H.-P., Deitmer, J. W., de Groot, B. L., and MacAulay, N. (2016). Aquaporin 4
 523 as a NH₃ Channel. *Journal of Biological Chemistry*, 291(36):19184–19195.
- 524 Bauer, S. and Ziv, E. (1976). Dense growth of aerobic bacteria in a bench-scale fermentor. *Biotechnology and
 525 Bioengineering*, 18(1):81–94. _eprint: <https://onlinelibrary.wiley.com/doi/10.1002/bit.260180107>.
- 526 Belliveau, N. M., Barnes, S. L., Ireland, W. T., Jones, D. L., Sweredoski, M. J., Moradian, A., Hess, S., Kinney, J. B., and
 527 Phillips, R. (2018). Systematic approach for dissecting the molecular mechanisms of transcriptional regulation
 528 in bacteria. *Proceedings of the National Academy of Sciences*, 115(21):E4796–E4805.
- 529 Birnbaum, L. S. and Kaplan, S. (1971). Localization of a Portion of the Ribosomal RNA Genes in *Escherichia coli*.
 530 *Proceedings of the National Academy of Sciences*, 68(5):925–929.
- 531 Booth, I. R., Mitchell, W. J., and Hamilton, W. A. (1979). Quantitative analysis of proton-linked transport systems.
 532 The lactose permease of *Escherichia coli*. *Biochemical Journal*, 182(3):687–696.
- 533 Bremer, H. and Dennis, P. P. (2008). Modulation of Chemical Composition and Other Parameters of the Cell at
 534 Different Exponential Growth Rates. *EcoSal Plus*, 3(1).
- 535 Browning, D. F. and Busby, S. J. W. (2016). Local and global regulation of transcription initiation in bacteria.
 536 *Nature Reviews Microbiology*, 14(10):638–650.
- 537 Dai, X., Zhu, M., Warren, M., Balakrishnan, R., Patsalo, V., Okano, H., Williamson, J. R., Fredrick, K., Wang, Y.-P.,
 538 and Hwa, T. (2016). Reduction of translating ribosomes enables *Escherichia coli* to maintain elongation rates
 539 during slow growth. *Nature Microbiology*, 2(2):16231.
- 540 Escalante, A., Salinas Cervantes, A., Gosset, G., and Bolívar, F. (2012). Current knowledge of the *Escherichia coli*
 541 phosphoenolpyruvate–carbohydrate phosphotransferase system: Peculiarities of regulation and impact on
 542 growth and product formation. *Applied Microbiology and Biotechnology*, 94(6):1483–1494.
- 543 Feist, A. M., Henry, C. S., Reed, J. L., Krummenacker, M., Joyce, A. R., Karp, P. D., Broadbelt, L. J., Hatzimanikatis, V.,
 544 and Palsson, B. Ø. (2007). A genome-scale metabolic reconstruction for *Escherichia coli* K-12 MG1655 that
 545 accounts for 1260 ORFs and thermodynamic information. *Molecular Systems Biology*, 3(1):121.
- 546 Fernández-Coll, L., Maciąg-Dorszynska, M., Tailor, K., Vadia, S., Levin, P. A., Szalewska-Palasz, A., Cashel, M., and
 547 Dunny, G. M. (2020). The Absence of (p)ppGpp Renders Initiation of *Escherichia coli* Chromosomal DNA
 548 Synthesis Independent of Growth Rates. *mBio*, 11(2):45.

- 549 Fijalkowska, I. J., Schaaper, R. M., and Jonczyk, P. (2012). DNA replication fidelity in *Escherichia coli*: A multi-DNA
550 polymerase affair. *FEMS Microbiology Reviews*, 36(6):1105–1121.
- 551 Finkelstein, I. J. and Greene, E. C. (2013). Molecular Traffic Jams on DNA. *Annual Review of Biophysics*, 42(1):241–
552 263.
- 553 Gama-Castro, S., Salgado, H., Santos-Zavaleta, A., Ledezma-Tejeida, D., Muñiz-Rascado, L., García-Sotelo, J. S.,
554 Alquicira-Hernández, K., Martínez-Flores, I., Pannier, L., Castro-Mondragón, J. A., Medina-Rivera, A., Solano-Lira,
555 H., Bonavides-Martínez, C., Pérez-Rueda, E., Alquicira-Hernández, S., Porrón-Sotelo, L., López-Fuentes, A.,
556 Hernández-Koutoucheva, A., Moral-Chávez, V. D., Rinaldi, F., and Collado-Vides, J. (2016). RegulonDB version
557 9.0: High-level integration of gene regulation, coexpression, motif clustering and beyond. *Nucleic Acids
558 Research*, 44(D1):D133–D143.
- 559 Ge, J., Yu, G., Ator, M. A., and Stubbe, J. (2003). Pre-Steady-State and Steady-State Kinetic Analysis of *E. coli* Class I
560 Ribonucleotide Reductase. *Biochemistry*, 42(34):10071–10083.
- 561 Goldman, S. R., Nair, N. U., Wells, C. D., Nickels, B. E., and Hochschild, A. (2015). The primary σ factor in *Escherichia
562 coli* can access the transcription elongation complex from solution *in vivo*. *eLife*, 4:e10514.
- 563 Harris, R. M., Webb, D. C., Howitt, S. M., and Cox, G. B. (2001). Characterization of PitA and PitB from *Escherichia
564 coli*. *Journal of Bacteriology*, 183(17):5008–5014.
- 565 Heldal, M., Norland, S., and Tumyr, O. (1985). X-ray microanalytic method for measurement of dry matter and
566 elemental content of individual bacteria. *Applied and Environmental Microbiology*, 50(5):1251–1257.
- 567 Ireland, W. T., Beeler, S. M., Flores-Bautista, E., Belliveau, N. M., Sweredoski, M. J., Moradian, A., Kinney, J. B., and
568 Phillips, R. (2020). Deciphering the regulatory genome of *Escherichia coli*, one hundred promoters at a time. *bioRxiv*.
- 570 Jacob, F. and Monod, J. (1961). Genetic regulatory mechanisms in the synthesis of proteins. *Journal of Molecular
571 Biology*, 3(3):318–356.
- 572 Jensen, R. B., Wang, S. C., and Shapiro, L. (2001). A moving DNA replication factory in *Caulobacter crescentus*.
573 *The EMBO journal*, 20(17):4952–4963.
- 574 Jun, S., Si, F., Pugatch, R., and Scott, M. (2018). Fundamental principles in bacterial physiology - history, recent
575 progress, and the future with focus on cell size control: A review. *Reports on Progress in Physics*, 81(5):056601.
- 576 Kapanidis, A. N., Margeat, E., Laurence, T. A., Doose, S., Ho, S. O., Mukhopadhyay, J., Kortkhonjia, E., Mekler, V.,
577 Ebright, R. H., and Weiss, S. (2005). Retention of Transcription Initiation Factor Σ 70 in Transcription Elongation:
578 Single-Molecule Analysis. *Molecular Cell*, 20(3):347–356.
- 579 Khademi, S., O'Connell, J., Remis, J., Robles-Colmenares, Y., Miercke, L. J. W., and Stroud, R. M. (2004). Mechanism
580 of Ammonia Transport by Amt/MEP/Rh: Structure of AmtB at 1.35 Å. *Science*, 305(5690):1587–1594.
- 581 Levin, B. R., McCall, I. C., Perrot, V., Weiss, H., Ovesepian, A., and Baquero, F. (2017). A Numbers Game: Ribosome
582 Densities, Bacterial Growth, and Antibiotic-Mediated Stasis and Death. *mBio*, 8(1).
- 583 Li, G.-W., Burkhardt, D., Gross, C., and Weissman, J. S. (2014). Quantifying absolute protein synthesis rates
584 reveals principles underlying allocation of cellular resources. *Cell*, 157(3):624–635.
- 585 Liebermeister, W., Noor, E., Flamholz, A., Davidi, D., Bernhardt, J., and Milo, R. (2014). Visual account of protein
586 investment in cellular functions. *Proceedings of the National Academy of Sciences*, 111(23):8488–8493.
- 587 Liu, M., Durfee, T., Cabrera, J. E., Zhao, K., Jin, D. J., and Blattner, F. R. (2005). Global Transcriptional Programs
588 Reveal a Carbon Source Foraging Strategy by *Escherichia coli*. *Journal of Biological Chemistry*, 280(16):15921–
589 15927.
- 590 Milo, R., Jorgensen, P., Moran, U., Weber, G., and Springer, M. (2010). BioNumbers—the database of key numbers
591 in molecular and cell biology. *Nucleic Acids Research*, 38(suppl_1):D750–D753.
- 592 Monod, J. (1947). The phenomenon of enzymatic adaptation and its bearings on problems of genetics and
593 cellular differentiation. *Growth Symposium*, 9:223–289.
- 594 Mooney, R. A., Darst, S. A., and Landick, R. (2005). Sigma and RNA Polymerase: An On-Again, Off-Again
595 Relationship? *Molecular Cell*, 20(3):335–345.

- 596 Mooney, R. A. and Landick, R. (2003). Tethering Σ 70 to RNA polymerase reveals high *in vivo* activity of σ factors
597 and Σ 70-dependent pausing at promoter-distal locations. *Genes & Development*, 17(22):2839–2851.
- 598 Neidhardt, F. C., Ingraham, J., and Schaechter, M. (1991). *Physiology of the Bacterial Cell - A Molecular Approach*,
599 volume 1. Elsevier.
- 600 Patrick, M., Dennis, P. P., Ehrenberg, M., and Bremer, H. (2015). Free RNA polymerase in *Escherichia coli*. *Biochimie*,
601 119:80–91.
- 602 Peebo, K., Valgepea, K., Maser, A., Nahku, R., Adamberg, K., and Vilu, R. (2015). Proteome reallocation in
603 *Escherichia coli* with increasing specific growth rate. *Molecular BioSystems*, 11(4):1184–1193.
- 604 Perdue, S. A. and Roberts, J. W. (2011). σ^{70} -dependent Transcription Pausing in *Escherichia coli*. *Journal of*
605 *Molecular Biology*, 412(5):782–792.
- 606 Phillips, R. (2018). Membranes by the Numbers. In *Physics of Biological Membranes*, pages 73–105. Springer,
607 Cham, Cham.
- 608 Ramos, S. and Kaback, H. R. (1977). The relation between the electrochemical proton gradient and active
609 transport in *Escherichia coli* membrane vesicles. *Biochemistry*, 16(5):854–859.
- 610 Rosenberg, H., Gerdes, R. G., and Chegwidde, K. (1977). Two systems for the uptake of phosphate in *Escherichia*
611 *coli*. *Journal of Bacteriology*, 131(2):505–511.
- 612 Rudd, S. G., Valerie, N. C. K., and Helleday, T. (2016). Pathways controlling dNTP pools to maintain genome
613 stability. *DNA Repair*, 44:193–204.
- 614 Sánchez-Romero, M. A., Molina, F., and Jiménez-Sánchez, A. (2011). Organization of ribonucleoside diphosphate
615 reductase during multifork chromosome replication in *Escherichia coli*. *Microbiology*, 157(8):2220–2225.
- 616 Schaechter, M., Maaløe, O., and Kjeldgaard, N. O. (1958). Dependency on Medium and Temperature of Cell Size
617 and Chemical Composition during Balanced Growth of *Salmonella typhimurium*. *Microbiology*, 19(3):592–606.
- 618 Schmidt, A., Kochanowski, K., Vedelaar, S., Ahrné, E., Volkmer, B., Callipo, L., Knoops, K., Bauer, M., Aebersold,
619 R., and Heinemann, M. (2016). The quantitative and condition-dependent *Escherichia coli* proteome. *Nature*
620 *Biotechnology*, 34(1):104–110.
- 621 Scholz, S. A., Diao, R., Wolfe, M. B., Fivenson, E. M., Lin, X. N., and Freddolino, P. L. (2019). High-Resolution
622 Mapping of the *Escherichia coli* Chromosome Reveals Positions of High and Low Transcription. *Cell Systems*,
623 8(3):212–225.e9.
- 624 Scott, M., Gunderson, C. W., Mateescu, E. M., Zhang, Z., and Hwa, T. (2010). Interdependence of cell growth and
625 gene expression: origins and consequences. *Science*, 330(6007):1099–1102.
- 626 Sekowska, A., Kung, H.-F., and Danchin, A. (2000). Sulfur Metabolism in *Escherichia coli* and Related Bacteria:
627 Facts and Fiction. *Journal of Molecular Microbiology and Biotechnology*, 2(2):34.
- 628 Si, F., Le Treut, G., Sauls, J. T., Vadia, S., Levin, P. A., and Jun, S. (2019). Mechanistic Origin of Cell-Size Control and
629 Homeostasis in Bacteria. *Current Biology*, 29(11):1760–1770.e7.
- 630 Si, F., Li, D., Cox, S. E., Sauls, J. T., Azizi, O., Sou, C., Schwartz, A. B., Erickstad, M. J., Jun, Y., Li, X., and Jun, S. (2017).
631 Invariance of Initiation Mass and Predictability of Cell Size in *Escherichia coli*. *Current Biology*, 27(9):1278–1287.
- 632 Sirko, A., Zatyka, M., Sadowy, E., and Hulanicka, D. (1995). Sulfate and thiosulfate transport in *Escherichia coli*
633 K-12: Evidence for a functional overlapping of sulfate- and thiosulfate-binding proteins. *Journal of Bacteriology*,
634 177(14):4134–4136.
- 635 Stasi, R., Neves, H. I., and Spira, B. (2019). Phosphate uptake by the phosphonate transport system PhnCDE.
636 *BMC Microbiology*, 19.
- 637 Stevenson, B. S. and Schmidt, T. M. (2004). Life History Implications of rRNA Gene Copy Number in *Escherichia*
638 *coli*. *Applied and Environmental Microbiology*, 70(11):6670–6677.
- 639 Svenningsen, S. L., Kongstad, M., Stenum, T. S. n., Muñoz-Gómez, A. J., and Sørensen, M. A. (2017). Transfer RNA
640 is highly unstable during early amino acid starvation in *Escherichia coli*. *Nucleic Acids Research*, 45(2):793–804.
- 641 Szenk, M., Dill, K. A., and de Graff, A. M. R. (2017). Why Do Fast-Growing Bacteria Enter Overflow Metabolism?
642 Testing the Membrane Real Estate Hypothesis. *Cell Systems*, 5(2):95–104.

- 643 Taheri-Araghi, S., Bradde, S., Sauls, J. T., Hill, N. S., Levin, P. A., Paulsson, J., Vergassola, M., and Jun, S. (2015).
644 Cell-size control and homeostasis in bacteria. - PubMed - NCBI. *Current Biology*, 25(3):385–391.
- 645 Taymaz-Nikerel, H., Borujeni, A. E., Verheijen, P. J. T., Heijnen, J. J., and van Gulik, W. M.
646 (2010). Genome-derived minimal metabolic models for *Escherichia coli* MG1655 with estimated
647 in vivo respiratory ATP stoichiometry. *Biotechnology and Bioengineering*, 107(2):369–381. _eprint:
648 <https://onlinelibrary.wiley.com/doi/pdf/10.1002/bit.22802>.
- 649 Valgepea, K., Adamberg, K., Seiman, A., and Vilu, R. (2013). *Escherichia coli* achieves faster growth by increasing
650 catalytic and translation rates of proteins. *Molecular BioSystems*, 9(9):2344.
- 651 van Heeswijk, W. C., Westerhoff, H. V., and Boogerd, F. C. (2013). Nitrogen Assimilation in *Escherichia coli*: Putting
652 Molecular Data into a Systems Perspective. *Microbiology and Molecular Biology Reviews*, 77(4):628–695.
- 653 Willsky, G. R., Bennett, R. L., and Malamy, M. H. (1973). Inorganic Phosphate Transport in *Escherichia coli*:
654 Involvement of Two Genes Which Play a Role in Alkaline Phosphatase Regulation. *Journal of Bacteriology*,
655 113(2):529–539.
- 656 Zhang, L., Jiang, W., Nan, J., Almqvist, J., and Huang, Y. (2014a). The *Escherichia coli* CysZ is a pH dependent
657 sulfate transporter that can be inhibited by sulfite. *Biochimica et Biophysica Acta (BBA) - Biomembranes*,
658 1838(7):1809–1816.
- 659 Zhang, Z., Aboulwafa, M., and Saier, M. H. (2014b). Regulation of crp gene expression by the catabolite
660 repressor/activator, cra, in *Escherichia coli*. *Journal of Molecular Microbiology and Biotechnology*, 24(3):135–141.
- 661 Zhu, M. and Dai, X. (2019). Growth suppression by altered (p)ppGpp levels results from non-optimal resource
662 allocation in *Escherichia coli*. *Nucleic Acids Research*, 47(9):4684–4693.